ACS OMEGA

http://pubs.acs.org/journal/acsodf

Article

cis-[6-(Pyridin-2-yl)-1,3,5-triazine-2,4-diamine](dichloride) Palladium(II)-Based Electrolyte Membrane Reactors for Partial Oxidation Methane to Methanol

Luis M. S. Garcia, Priscilla J. Zambiazi,* Khaoula Chair, Tuan Duy Doan, Andrezza S. Ramos, Julio Nandenha, Rodrigo F. B. De Souza, Larissa Otubo, Adam Duong, and Almir O. Neto

Cite This: *ACS Omega* 2022, 7, 24249−24255

Read Online

ACCESS | Metrics & More | Article Recommendations | Supporting Information

ABSTRACT: Methane is an abundant resource and the main constituent of natural gas. It can be converted into higher value-added products and as a subproduct of electricity co-generation. The application of polymer electrolyte reactors for the partial oxidation of methane to methanol to co-generate power and chemical products is a topic of great interest for gas and petroleum industries, especially with the use of materials with a lower amount of metals, such as palladium complex. In this study, we investigate the ideal relationship between *cis*-[6-(pyridin-2-yl)-1,3,5-triazine-2,4-diamine(dichloride)-palladium(II)] (Pd-complex) nanostructure and carbon to obtain a stable, conductive, and functional reagent diffusion electrode. The physical and structural properties of the material were analyzed by Fourier transform infrared (FT-IR) and Raman spectroscopies, transmission electron microscopy (TEM), and X-ray powder diffraction (XRD) techniques. The electrocatalytic activity studies revealed that the most active proportion was 20% of Pd-complex supported on carbon (m/m), which was measured with lower values of open-circuit and power density but with higher efficiency in methanol production with reaction rates of r = 4.2 mol $L^{-1}{\cdot}h^{-1}$ at 0.05 V.

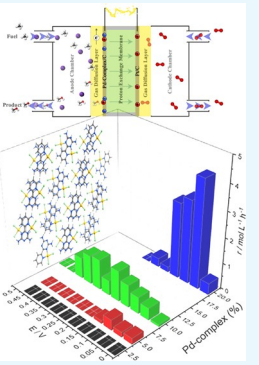

INTRODUCTION

Direct partial oxidation of methane to methanol is a hot topic for gas industries and a great challenge in the areas of catalysis and energy.[1] Methane is the major component of natural gas. In the oil and gas industries, methane is combusted to produce energy for the extraction process. The combustion is also a quick method to eliminate the gas. Approximately 145 billion square meters of this natural gas per year is produced, and the majority is used for thermal power generation, thus generating around 1% of the global carbon dioxide emissions.[1] The conversion of methane into value-added chemicals and fuels such as methanol is thus highly desirable. Partial oxidation of CH_4 gas to MeOH liquid is one of the most promising alternatives to exploit this abundant energy resource and facilitate its transport. Nowadays, due to the emerging energy applications, the demand for methanol is over a few tens of million cubic tons per year.[2]

Currently, available technologies to produce methanol from methane involve a two-step process, namely, the steam reforming of CH_4 to syngas at 850 °C and its subsequent catalytic conversion to MeOH.[3] Steam reforming is the most energy-consuming and expensive process. To generate sufficient profit, it is primordial for industries to develop new synthetic routes. The development of direct conversion of CH_4 to MeOH under ambient conditions to offer a sustainable way for the efficient use of natural resources such as natural gas, shale gas, and biogas is a great goal.[4] Bearing this in mind, scientists have made tremendous efforts to develop methods to produce MeOH. Presently, the electrochemical process using polymer electrolyte reactor-fuel cell type (PER-FC) for partial oxidation of methane in one step under mild conditions (∼80 °C or less) is one of the most successful methods because of the possibility to operate in electrolytic and galvanic modes under continuous flow to simultaneously produce methanol and energy co-generation.[5−9] Low-temperature operation is interesting to avoid warm-up time (quick start) and reduces deterioration of system components.

However, there are still many other drawbacks that need to be changed before reaching an efficient and inexpensive PER-FC technology. One of the disadvantages of the technology is the use of noble metals (platinum, platinum alloys, etc.) as catalysts thus adding to system cost.[5,8,10] Furthermore, platinum is also extremely sensitive to carbon dioxide poisoning, which obliges the addition of extra reactors to separate CO_2 from the fuel gas.

Recently, palladium has been reported as a promising metal for partial oxidation of methane due to the formation of a thin layer of PdO on the catalytic surface, which displays an affinity

Received: March 10, 2022
Accepted: May 20, 2022
Published: July 5, 2022

Scheme 1. Diagram of the PER-FC Electrochemical System

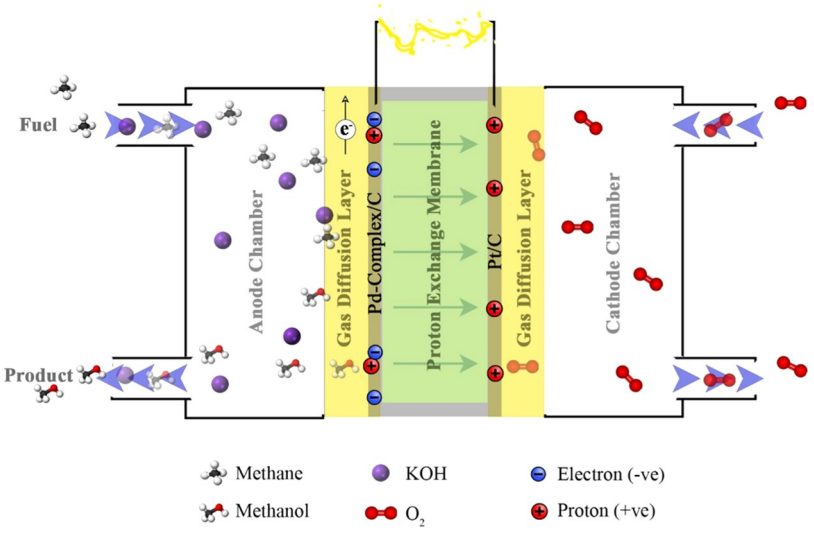

with methane and the oxy-hydroxide species at a low overpotential that can activate the water, an important step for hydrocarbon oxidation.[10−13] However, the price of Pd metal has increased over the last few years. Meanwhile, the metal−ligand complex has gained increasing attention as electrocatalysts due to the lower proportion of metals; these materials have a large specific surface area and high porosity and are readily available.[14−18] In this sense, electrocatalysts based on macrocyclic, linear, and multidentate ligands N-coordinated to transition metals have been explored in fuel cells.[19−24]

In our previous report, we have demonstrated that the chemicals and the power from methane can be co-generated using PER-FC with [6,6′-(2,2′-bipyridine-6,6′-diyl)*bis*(1,3,5-triazine-2,4-diamine)(nitrate-*O*)copper(II)] complex as a catalyst.[9] Here, we investigated the conversion of methane to methanol using the *cis*-[6-(pyridin-2-yl)-1,3,5-triazine-2,4-diamine(dichloride)palladium(II)] (Pd-complex) in an anode of PER-FC type for the conversion of methane to methanol. Our objective is to study the catalytic activity of Pd-complex using PER-FC to convert CH_4 into MeOH. The use of Pd-complex as a catalyst can be advantageous due to the known adsorption capacity of methane on oxidized Pd nodes with the characteristics of organometallic complexes, in addition to reducing the amount of metal expended for its works. Besides, the strategy to use these compounds to drive the electrocatalytic methanol formation was due to the molecular structure of the Pd(II) complex presenting bidentate triazine-pyridine ligand N-donor atoms, and the ligand chelates to form a five-membered ring with characteristic strong electron donors ensuring stability to the complex due to its resonant character. Besides, the stereochemical environment of the Pd(II) complex is favorable since the structure presents quadratic geometry with greater exposure of the metallic center, suggesting a potential precursor for heterogeneous catalytic processes.[25]

EXPERIMENTAL SECTION

Pd-complex was obtained by reacting the pre-ligand 6-(pyridin-2-yl)-1,3,5-triazine-2,4-diamine (1 equiv) with the metal salt $PdCl_2$ (1 equiv) in acetonitrile according to the known method.[26] The electrocatalyst was prepared by mechanically mixing the Pd-complex with Vulcan carbon in proportions of 1, 2.5, 5, 10, and 20% (mass/mass). The physical and chemical characterizations of the Pd-complex were performed using Fourier transform infrared (FT-IR) and Raman spectroscopies. The crystalline structure was confirmed by X-ray powder diffraction (XRD) using a Miniflex II diffractometer, with a Cukα radiation source of 0.15406 Å, regulated in the range of 2θ = 2−90°, with a scan speed of 2 min^{-1}. A JEOL JEM-2100 electron microscope operated at 200 kV was used to determine the morphology and nanostructure of the Pd-complex particles.

All electrochemical activities using polymeric electrolytic reactor-fuel cell type (PER-FC) for partial oxidation of methane are well described in the literature.[9,11,27,28] The electrochemical measurements were performed using a three-electrode cell, Ametek PARSTAT 3000A-DXbi-potentiostat/galvanostat. In the conventional electrochemical cell, Ag/AgCl and Pt were used as the reference electrode and counter electrode (area = 2 cm^2), respectively. Aliquots of 15 μL of each sample were added to the working electrodes, which consisted of a previously prepared ink composed of a mixture of 8 mg of catalyst, 750 μL of H_2O, 250 μL of isopropyl alcohol, and 15 μL of 5% Nafion D-520. All experiments with different percentages of the Pd-complex were carried out in an aqueous solution of KOH 1 mol·L^{-1}.

To perform the PER-FC tests and obtain the polarization curves, the membrane electrode (MEA) was mounted with a Nafion 117 membrane doped with KOH. BASF Pt/C catalyst (20% by weight) with 1 mg·cm^{-2} was used as the cathode in gas diffusion electrodes, and catalysts with different Pd-complex ratios served as the anode. The reactor, a stainless-steel cell-type with serpentine to distribution, was fed with CH_4 at a flow rate of 50 mL·min^{-1} and 1.0 mol·L^{-1} KOH solution at a flow rate of 1 mL·min^{-1} at ambient temperature at the anode. In the cathodic chamber, it was fed with external O_2 with the aid of a humidifier bottle with a controlled temperature of 80 °C with a flow rate of 200 mL·min^{-1}. Scheme 1 shows the diagram of the polymer electrolytic reactor-fuel cell (PER-FC) system for the partial oxidation of methane to methanol.

Fourier transform infrared (FT-IR) spectroscopy was used to determine the different species formed during the

https://doi.org/10.1021/acsomega.2c01463
ACS Omega 2022, 7, 24249−24255

electrochemical oxidation of methane in an alkaline medium at different potentials. Anodic reaction products were collected at 300 s increments of 50 mV and analyzed by attenuated total reflectance Fourier transform infrared (ATR-FT-IR) spectroscopy performed on an ATR accessory (MIRacle with ZnSe Crystal Plate Pike) installed on a Nicolet 6700 FT-IR spectrometer equipped with an MCT detector and cooled with liquid N_2. Raman spectroscopy was used for the characterization and quantitative determination of the products obtained using Horiba Scientific MacroRam Raman spectroscopy equipment, using a wavelength fixed at 785 nm. The concentration of methanol obtained from the solutions collected in the effluent of the polymeric membrane reactor was determined by the method described by Boyaci et al.[29]

RESULTS AND DISCUSSION

The physical characterizations of the nanostructure palladium complex were performed to determine its morphological, crystallographic, and surface state structures. Figure 1 shows

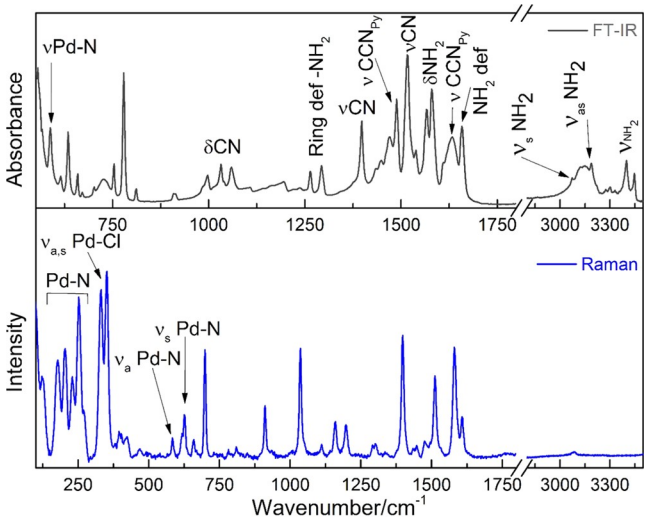

Figure 1. FT-IR and Raman spectra of the cis-square planar Pd-complex.

the FT-IR and Raman spectra that were used to determine their structural properties. From the FT-IR spectrum, it is possible to observe the characteristic bands of the bidentate ligand of the Pd-complex, referring to the triazine and pyridine groups, and showing good agreement with the literature.[30−33] Symmetrical and asymmetrical stretches of the amine group linked to the aromatic ring triazines are confirmed in regions of 3069 and 3193 cm^{-1}, respectively. The coordination of the N atom to the metallic center of Pd, on the other hand, can be characterized by the stretch ν(Pd−N) in 587 cm^{-1}, while the Pd−Cl bond is found in the low-frequency regions of the spectrum. The Pd-complex with square planar geometry of *cis* conformation shows a characteristic Raman spectrum,[34,35] and the bands due to metal−halogen vibration are at a low frequency and have high intensity found at wavenumbers 331 and 351 cm^{-1}. However, the chelated form of Pd-complex, N−Pd−N, can be confirmed by symmetric and asymmetric stretches at 585 and 629 cm^{-1}, respectively.[36] Furthermore, Pd−N binding is evidenced by bands in the low-frequency regions, as shown in the spectrum.

The nanostructure of the Pd-complex was analyzed by transmission electron microscopy (TEM) and X-ray powder diffraction techniques. Figure 2A shows the cluster of nanoparticles of the Pd-complex. At a higher magnification, the micrograph (Figure 2B) shows periodic fringed folds with a *d*-spacing between the crystallographic planes (002), (111), and (004) of approximately 0.761, 0.514, and 0.381 nm, respectively, which can be attributed to the organization of the solid-state Pd-complex as reported by Duong et al.[26] To facilitate the observation of the analogy between the TEM image and the crystallographic data, a view of the structure of Pd-complex is presented succinctly in Figure 2C,D. As determined from the single-crystal X-ray diffraction (SCXRD), the Pd-complex crystal structure is formed by two-dimensional (2D) π-stacking interactions, and hydrogen bonds join these two-dimensional columns together to form a three-dimensional (3D) structure that is further stacked to generate the layer structure. From the XRD powder (Figure 3), the *d*-spacing between layers is in good agreement with the value determined by TEM. The diffraction pattern obtained experimentally corresponds to the pattern calculated from the crystal structure obtained by single-crystal refinement. The diffraction pattern shows the planes corresponding to the diffraction angles, and the distances between the planes were correlated with those obtained through TEM analysis.

Figure 4 shows the cyclic voltammetry of the catalyst in several mass ratios of Pd-complex. As can be seen, the reduction peak at −0.32 V shifts to a higher potential with the increase of the percentage of Pd-complex.[37] For Pd-complex 20%, the shift is much more important. This observation can be assigned to the reduction of palladium species.[2] Furthermore, a small peak at 0.01 V is notable, indicating the formation of palladium oxides or surfaces containing palladium.[2,11]

Figure 5 presents the electrochemical curves of PER-FC for different Pd-complex/carbon proportions with KOH and methane introduced on the anode. In this figure, it is possible to observe that electrocatalyst in a higher amount of Pd-complex shows a lower value of open-circuit voltage (OCV). The composite with 10% of the Pd-complex is the one that displays the biggest open-circuit value and power density compared to the other catalysts. The values of OCVs obtained for all Pd-complex/C (∼0.27−0.5 V) are similar to those reported in the literature that contains palladium systems (ca. 0.2−0.4 V).[1,9,10] The higher OCV values measured in our case can be explained by the formation of methanol or formates close to onset potential, and/or lower potential of water activation.

Figure 6 shows the IR spectra of PER-FC effluent to detect the products obtained during the operation. Spectra obtained for all materials display the deg deform band characteristic of the methane at ∼1308 cm^{-1}.[38,39] It is known that methane is poorly soluble in water, but its solubility greatly increases with the presence of the other organic compounds in the solution.[10] In the alkaline medium, three species (methanol, formates, and carbonates) are observed during the partial oxidation of methane. Methanol was detected with the bands at 1033, 1078, and 1482 cm^{-1}.[10,40] Its formation is observed at a potential close to the OCV. The presence of formate molecules is noted with the bands at 1337 cm^{-1} attributed to ν(COO).[41] This compound is principally formed with the Pd-complex 2.5% catalyst. The quantity of formate generated increases near OCV. For Pd-complexes 10 and 20%, the formate is formed at

https://doi.org/10.1021/acsomega.2c01463
ACS Omega 2022, 7, 24249−24255

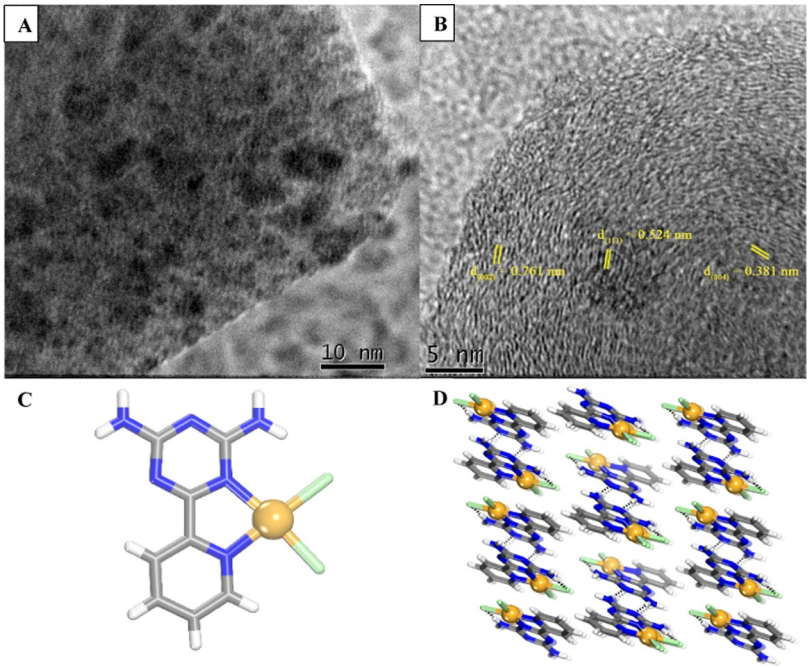

Figure 2. TEM micrographs obtained from Pd-complex electrocatalysts in different magnifications: (A) 10 nm and (B) 5 nm with the d-spacing planar of the cluster's nanostructure polycrystalline. (C) cis-Square planar molecular structure of the Pd-complex and (D) crystalline structure viewing along the *c* axis. The view shows how single molecules are linked together by hydrogen bonds to form chains and further stacked to produce 2D-layer packing.

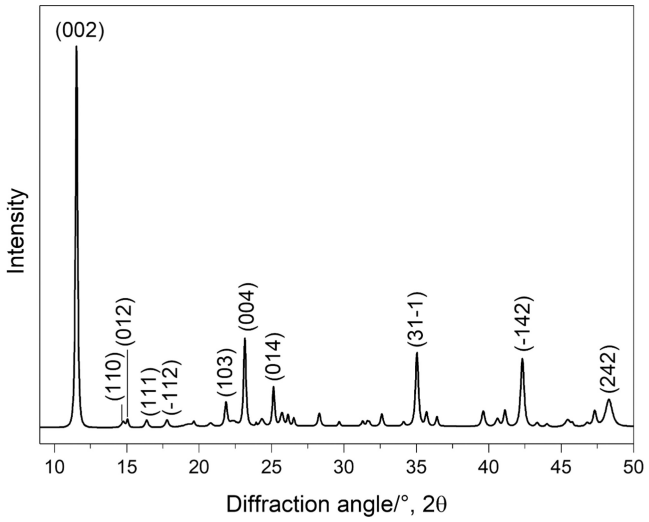

Figure 3. X-ray powder diffraction (XRD) pattern of the polycrystalline Pd-complex with the crystallographic planes.

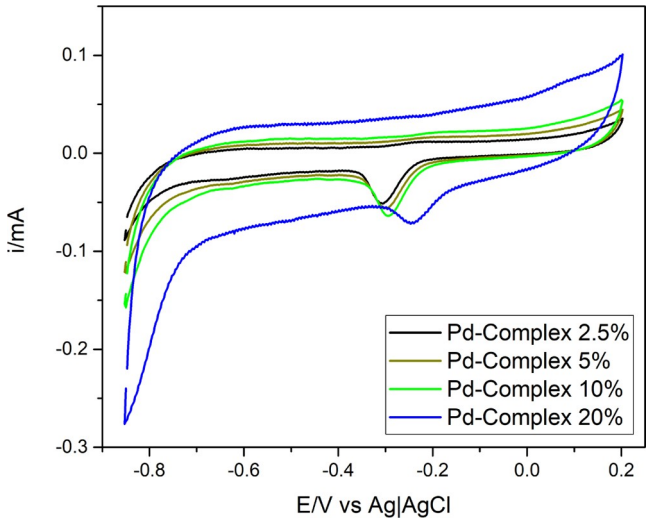

Figure 4. Cyclic voltammetry of Pd-complex/carbon Vulcan material in 1 mol·L^{-1} KOH (ν = 10 mV·s^{-1}).

a potential of 0.25 V and lower. The carbonate is observed at ∼1380 cm^{-1},[42,43] in the case of Pd-complex 2.5%. For Pd-complex 10%, this band appears for all potentials. In the case of Pd-complex 20%, carbonate molecules are not detected at all.

The activity of catalysts for the conversion of methane into methanol is measured by the number of molecules converted as a function of time, for which the reaction rate (r) (eq 1) is an important parameter to be evaluated. Figure 7 presents the correlation between the different potentials E and rates r for each ratio of Pd-complex to produce methanol. The r-value is calculated by eq 1, where the amount of methanol was quantified by Boyaci's method[29] determined by the Raman spectra for the construction of the analytical curve in the concentration range of 0.005−1.000 mol·L^{-1} of methanol (Figure S1). For the following analytical curve, an intensity of 33.886 + 32.377 [methanol][44] is obtained with the correlation coefficient being R^2 = 0.94252.

$$r = \frac{\text{methanol}_{\text{amount}}}{\text{volume} \times \text{time}} \quad (1)$$

The reaction rate for methanol production indicates that Pd-complex 20% (blue) is the most active composition, at 0.05−0.15 V with an r maximum of 4.2 mol·L^{-1}·h^{-1} at 0.05 V. The methane-to-methanol conversion ratio is around 4 times higher than the composition Pd-complex 10% (green). For Pd-complexes 5% (red) and 2.5% (black), small and no appreciable amounts of methanol were detected, respectively.

https://doi.org/10.1021/acsomega.2c01463
ACS Omega 2022, 7, 24249−24255

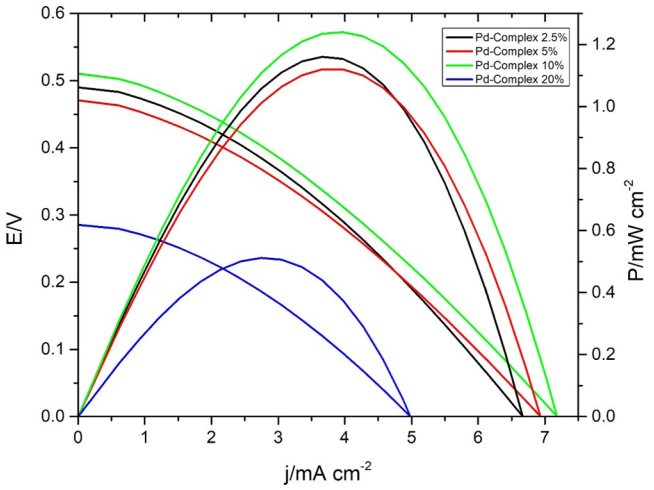

Figure 5. Polarization and power density curves of a 5 cm^2 SEMR-FC at room temperature using Pd-complex/carbon Vulcan catalyst anodes (5 $mg{\cdot}cm^{-2}$ catalyst loading) and Pt/C BASF as the cathode in all experiments (1 $mg{\cdot}cm^{-2}$ Pt catalyst loading with 20 wt % Pt loading on carbon), Nafion 117 membrane treated with KOH 1.0 $mol{\cdot}L^{-1}$ + CH_4 at 50 $mL{\cdot}min^{-1}$, and O_2 flux at 200 $mL{\cdot}min^{-1}$.

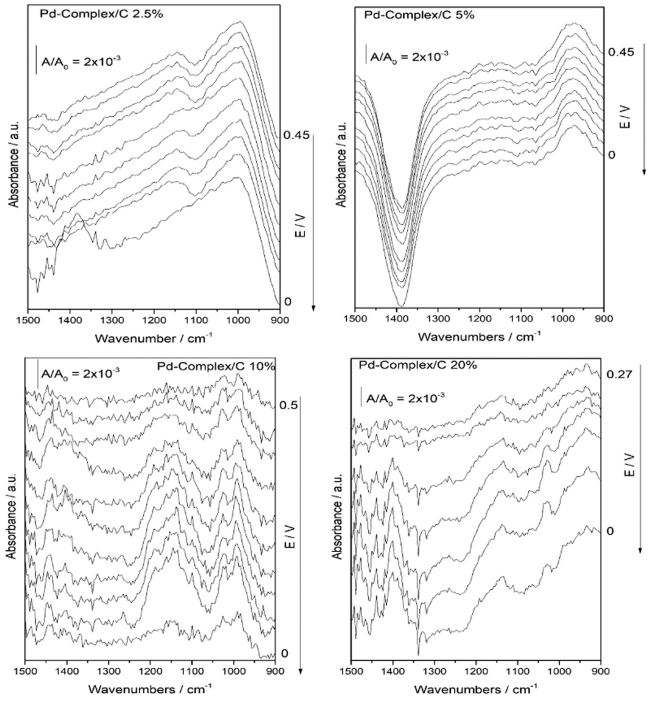

Figure 6. FT-IR spectra of the effluent of the PER-FC at several potentials in 1.0 $mol{\cdot}L^{-1}$ KOH, and the methane flow was set to 50 $mL{\cdot}min^{-1}$ for the Pd-complex.

These results corroborate the process that took place in the fuel cell chamber, in which water is activated at low overpotentials, provided by the complex that operates synergistically with the adsorption capacity of methane on Pd(II). As reported by Jin et al.[45] and Santos et al.,[10] the mechanism starts with the immobilization of the hydrocarbon so that it reacts with the products resulting from the water activation. The results show a greater activity for the composition with a higher amount of Pd-complex, which can be perceived by the formed products and the profiles observed by the *r* factor. However, it is possible that the reaction

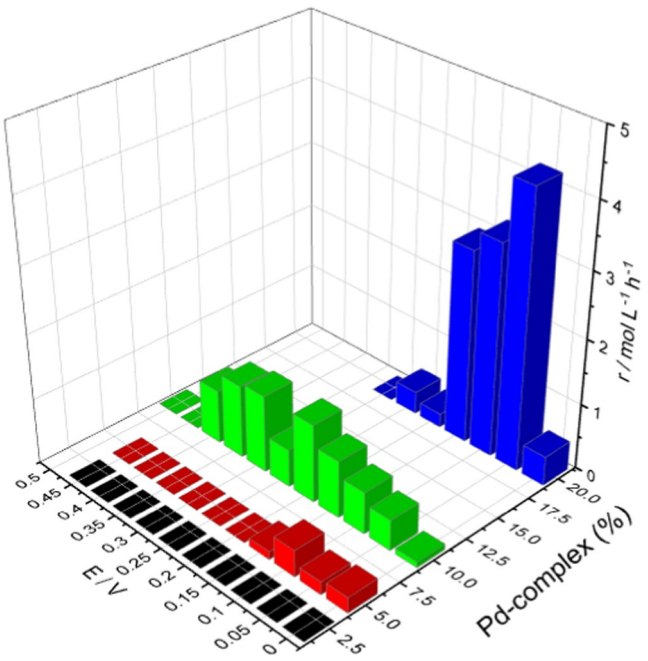

Figure 7. Reaction rate of methanol production in an SEMR-FC as a function of potential.

pathways have changed and therefore affected energy co-generation as shown in Figure 5.

CONCLUSIONS

The use of the Pd-complex/carbon electrocatalyst as an anode in the PER-FC reactor for converting methane into value-added chemical products with co-generation of energy is promising. The physical properties of the nanostructure Pd-complex were analyzed by FT-IR and Raman spectroscopy, and the structural properties were determined by imaging and polycrystal X-ray diffraction techniques. It is observed that the nanostructure formed by nanolayers from π-stacking interaction results in a cluster of grains formed by wrinkles and folds with *d*-spacing reticles between the crystallographic planes determined by the diffraction pattern. Pd-complex/carbon Vulcan materials display catalytic activity for the conversion of methane into methanol, formate, and carbonate. Our investigation is demonstrated by FT-IR spectroscopy and quantified by Raman spectroscopy that only ratios higher than 5% of Pd-complex are active to produce a detectable quantity of methanol. The catalyst with 20% with r = 4.2 $mol{\cdot}L^{-1}{\cdot}h^{-1}$ at 0.05 V displays the best parameters for an effective generation of methanol from methane.

ASSOCIATED CONTENT

Supporting Information

The Supporting Information is available free of charge at https://pubs.acs.org/doi/10.1021/acsomega.2c01463.

Raman spectra used for the calibration curve for methanol quantification (PDF)

AUTHOR INFORMATION

Corresponding Author

Priscilla J. Zambiazi − *Instituto de Pesquisas Energéticas e Nucleares, IPEN/CNEN−SP, CEP 05508-000 São Paulo,*

https://doi.org/10.1021/acsomega.2c01463
ACS Omega 2022, 7, 24249−24255

SP, Brazil; orcid.org/0000-0002-4371-4113; Email: pzambiazi@gmail.com

Authors

Luis M. S. Garcia − *Instituto de Pesquisas Energéticas e Nucleares, IPEN/CNEN−SP, CEP 05508-000 São Paulo, SP, Brazil; Département de Chimie, Biochimie et Physique, Institut de Recherchesur l'Hydrogène, Université du Québec a Trois-Rivières, Trois-Rivières, Québec G9A5H7, Canada*

Khaoula Chair − *Département de Chimie, Biochimie et Physique, Institut de Recherchesur l'Hydrogène, Université du Québec a Trois-Rivières, Trois-Rivières, Québec G9A5H7, Canada*

Tuan Duy Doan − *Département de Chimie, Biochimie et Physique, Institut de Recherchesur l'Hydrogène, Université du Québec a Trois-Rivières, Trois-Rivières, Québec G9A5H7, Canada*

Andrezza S. Ramos − *Instituto de Pesquisas Energéticas e Nucleares, IPEN/CNEN−SP, CEP 05508-000 São Paulo, SP, Brazil*

Julio Nandenha − *Instituto de Pesquisas Energéticas e Nucleares, IPEN/CNEN−SP, CEP 05508-000 São Paulo, SP, Brazil*

Rodrigo F. B. De Souza − *Instituto de Pesquisas Energéticas e Nucleares, IPEN/CNEN−SP, CEP 05508-000 São Paulo, SP, Brazil;* orcid.org/0000-0003-1501-1274

Larissa Otubo − *Instituto de Pesquisas Energéticas e Nucleares, IPEN/CNEN−SP, CEP 05508-000 São Paulo, SP, Brazil*

Adam Duong − *Département de Chimie, Biochimie et Physique, Institut de Recherchesur l'Hydrogène, Université du Québec a Trois-Rivières, Trois-Rivières, Québec G9A5H7, Canada;* orcid.org/0000-0002-4927-3603

Almir O. Neto − *Instituto de Pesquisas Energéticas e Nucleares, IPEN/CNEN−SP, CEP 05508-000 São Paulo, SP, Brazil*

Complete contact information is available at: https://pubs.acs.org/10.1021/acsomega.2c01463

Funding

The authors are grateful to CAPES, CNPq (302709/2020-7), FAPESP (2014/09087-4, 2014/50279-4, and 2017/11937-4) and CINE-SHELL (ANP) for financial support, the Natural Sciences and Engineering Research Council of Canada (RGPIN-2015-06425), the Canada Foundation for Innovation (37843), a support program for the internationalization of research, Emerging Leaders in the Americas Program, and the Université du Québec à Trois-Rivières for financial support.

Notes

The authors declare no competing financial interest.

REFERENCES

(1) Nandenha, J.; Nagahama, I.; Yamashita, J.; Fontes, E.; Ayoub, J.; de Souza, R.; Fonseca, F.; Neto, A. O. Activation of methane on PdZn/C electrocatalysts in an acidic electrolyte at low temperatures. *Int. J. Electrochem. Sci.* **2019**, *14*, 10819−10834.

(2) Omasta, T. J.; Peng, X.; Miller, H. A.; Vizza, F.; Wang, L.; Varcoe, J. R.; Dekel, D. R.; Mustain, W. E. Beyond 1.0 W cm−2Performance without Platinum: The Beginning of a New Era in Anion Exchange Membrane Fuel Cells. *J. Electrochem. Soc.* **2018**, *165*, J3039−J3044.

(3) Vo, T. H.; Shekhirev, M.; Kunkel, D. A.; Orange, F.; Guinel, M. J.; Enders, A.; Sinitskii, A. Bottom-up solution synthesis of narrow nitrogen-doped graphene nanoribbons. *Chem. Commun.* **2014**, *50*, 4172−4174.

(4) Li, S.; Ahmed, R.; Yi, Y.; Bogaerts, A. Methane to Methanol through Heterogeneous Catalysis and Plasma Catalysis. *Catalysts* **2021**, *11*, No. 590.

(5) Lee, B.; Hibino, T. Efficient and selective formation of methanol from methane in a fuel cell-type reactor. *J. Catal.* **2011**, *279*, 233−240.

(6) Zakaria, Z.; Kamarudin, S. K. Direct conversion technologies of methane to methanol: An overview. *Renewable Sustainable Energy Rev.* **2016**, *65*, 250−261.

(7) Pan, Z. F.; Chen, R.; An, L.; Li, Y. S. Alkaline anion exchange membrane fuel cells for cogeneration of electricity and valuable chemicals. *J. Power Sources* **2017**, *365*, 430−445.

(8) Alcaide, F.; Cabot, P.-L.; Brillas, E. Fuel cells for chemicals and energy cogeneration. *J. Power Sources s* **2006**, *153*, 47−60.

(9) Garcia, L. M. S.; Rajak, S.; Chair, K.; Godoy, C. M.; Silva, A. J.; Gomes, P. V. R.; Sanches, E. A.; Ramos, A. S.; De Souza, R. F. B.; Duong, A.; Neto, A. O. Conversion of Methane into Methanol Using the [6,6′-(2,2′-Bipyridine-6,6′-Diyl)bis(1,3,5-Triazine-2,4-Diamine)]-(Nitrato-O)Coppe r(II) Complex in a Solid Electrolyte Reactor Fuel Cell Type. *ACS Omega* **2020**, *5*, 16003−16009.

(10) Santos, M. C. L.; Nunes, L. C.; Silva, L. M. G.; Ramos, A. S.; Fonseca, F. C.; de Souza, R. F. B.; Neto, A. O. Direct Alkaline Anion Exchange Membrane Fuel Cell to Converting Methane into Methanol. *ChemistrySelect* **2019**, *4*, 11430−11434.

(11) Godoi, C. M.; Santos, M. C. L.; Silva, A. J.; Tagomori, T. L.; Ramos, A. S.; de Souza, R. F. B.; Neto, A. O. Methane conversion to higher value-added product and energy co-generation using anodes OF PdCu/C in a solid electrolyte reactor: alkaline fuel cell type monitored by differential mass spectroscopy. *Res. Chem. Intermed.* **2021**, *47*, 743−757.

(12) Stotz, H.; Maier, L.; Boubnov, A.; Gremminger, A. T.; Grunwaldt, J. D.; Deutschmann, O. Surface reaction kinetics of methane oxidation over PdO. *J. Catal.* **2019**, *370*, 152−175.

(13) Arminio-Ravelo, J. A.; Escudero-Escribano, M. Strategies toward the sustainable electrochemical oxidation of methane to methanol. *Curr. Opin. Green Sustainable Chem.* **2021**, *30*, No. 100489.

(14) Zhao, X.; Pachfule, P.; Thomas, A. Covalent organic frameworks (COFs) for electrochemical applications. *Chem. Soc. Rev.* **2021**, *50*, 6871−6913.

(15) You, J.; Zhao, Y.; Wang, L.; Bao, W. Recent developments in the photocatalytic applications of covalent organic frameworks: A review. *J. Cleaner Prod.* **2021**, *291*, No. 125822.

(16) Windle, C. D.; Perutz, R. N. Advances in molecular photocatalytic and electrocatalytic CO2 reduction. *Coord. Chem. Rev.* **2012**, *256*, 2562−2570.

(17) Gu, S.; Marianov, A. N.; Zhu, Y.; Jiang, Y. Cobalt porphyrin immobilized on the TiO2 nanotube electrode for CO2 electro-reduction in aqueous solution. *J. Energy Chem.* **2021**, *55*, 219−227.

(18) Gao, D.; Liu, T.; Wang, G.; Bao, X. Structure Sensitivity in Single-Atom Catalysis toward CO2 Electroreduction. *ACS Energy Lett.* **2021**, *6*, 713−727.

(19) Xu, M.; Ge, J.; Liu, C.; Xing, W. Recent advances in active sites identification and new M−N−C catalysts development towards ORR. *J. Phys. Mater.* **2021**, *4*, No. 044008.

(20) Idrees, M. Z.; Ilahi, I.; Ali, M. Z.; Muhammad, Z. Efficient palladium (II) electrocatalysts with thiophene anchored pyridinium amidates for CO2 reduction. *J. CO2 Util.* **2021**, *44*, No. 101384.

(21) Savastano, M.; Passaponti, M.; Giurlani, W.; Lari, L.; Calisi, N.; Delgado-Pinar, E.; Serrano, E. S.; Garcia-España, E.; Innocenti, M.; Lazarov, V. K.; Bianchi, A. Linear, tripodal, macrocyclic: Ligand geometry and ORR activity of supported Pd(II) complexes. *Inorg. Chim. Acta* **2021**, *518*, No. 120250.

(22) Therrien, J. A.; Wolf, M. O.; Patrick, B. O. Electrocatalytic Reduction of CO2 with Palladium Bis-N-heterocyclic Carbene Pincer Complexes. *Inorg. Chem.* **2014**, *53*, 12962−12972.

(23) Belenov, S. V.; Guterman, V. E.; Popov, L. D.; Kozakov, A. T.; Nikolsky, A. V.; Danilenko, M. V.; Safronenko, O. I.; Nikulin, A. Y. The study of the pyrolysis products of Ni (II) and Pd (II) chelate

complexes as catalysts for the oxygen electroreduction reaction. *J. Solid State Electrochem.* **2021**, *25*, 789−796.
(24) Savastano, M.; Passaponti, M.; Giurlani, W.; Lari, L.; Bianchi, A.; Innocenti, M. Multi-Walled Carbon Nanotubes Supported Pd(II) Complexes: A Supramolecular Approach towards Single-Ion Oxygen Reduction Reaction Catalysts. *Energies* **2020**, *13*, No. 5539.
(25) Sinha, S.; Mirica, L. M. Electrocatalytic O2 Reduction by an Organometallic Pd(III) Complex via a Binuclear Pd(III) Intermediate. *ACS Catal.* **2021**, *11*, 5202−5211.
(26) Duong, A.; Maris, T.; Wuest, J. D. Using Pyridinyl-Substituted Diaminotriazines to Bind Pd(II) and Create Metallotectons for Engineering Hydrogen-Bonded Crystals. *Inorg. Chem.* **2011**, *50*, 5605−5618.
(27) de Moura Souza, F.; de Souza, R. F. B.; Batista, B. L.; dos Santos, M. C.; Fonseca, F. C.; Neto, A. O.; Nandenha, J. Methane activation at low temperature in an acidic electrolyte using PdAu/C, PdCu/C, and PdTiO2/C electrocatalysts for PEMFC. *Res. Chem. Intermed.* **2020**, *46*, 2481−2496.
(28) Ramos, A. S.; Santos, M. C. L.; Godoi, C. M.; Oliveira Neto, A.; De Souza, R. F. B. Obtaining C2 and C3 Products from Methane Using Pd/C as Anode in a Solid Fuel Cell-type Electrolyte Reactor. *ChemCatChem* **2020**, *12*, 4517−4521.
(29) Boyaci, I. H.; Genis, H. E.; Guven, B.; Tamer, U.; Alper, N. A novel method for quantification of ethanol and methanol in distilled alcoholic beverages using Raman spectroscopy. *J. Raman Spectrosc.* **2012**, *43*, 1171−1176.
(30) Durig, J. R.; Layton, R.; Sink, D. W.; Mitchell, B. R. Far infrared spectra of palladium compounds−I. The influence of ligands upon the palladium chloride stretching frequency. *Spectrochim. Acta* **1965**, *21*, 1367−1378.
(31) Dikmen, G.; Hür, D. Palladium (II) complex: Synthesis, spectroscopic studies and DFT calculations. *Chem. Phys. Lett.* **2019**, *716*, 49−60.
(32) Yuan, X.; Luo, K.; Zhang, K.; He, J.; Zhao, Y.; Yu, D. Combinatorial Vibration-Mode Assignment for the FTIR Spectrum of Crystalline Melamine: A Strategic Approach toward Theoretical IR Vibrational Calculations of Triazine-Based Compounds. *J. Phys. Chem. A* **2016**, *120*, 7427−7433.
(33) Al-Khodir, F. A. I.; Abumelha, H. M. A.; Al-Warhi, T.; Al-Issa, S. A. New Platinum(IV) and Palladium(II) Transition Metal Complexes of s-Triazine Derivative: Synthesis, Spectral, and Anticancer Agents Studies. *Biomed. Res. Int.* **2019**, *2019*, No. 9835745.
(34) Roberto Pioquinto-Mendoza, J.; Martínez-Otero, D.; Andrade-López, N.; Alvarado-Rodríguez, J. G.; Salazar-Pereda, V.; Sánchez-Cabrera, G.; Zuno-Cruz, F. J. cis-Dichloro complexes of NiII, PdII, and PtII derived from 2-pyridylmethyl-N-substituted imines. *Polyhedron* **2013**, *50*, 289−296.
(35) Degen, I. A.; Rowlands, A. J. The Fourier transform Raman spectra of a series of platinum(II), palladium(II) and gold(III) square-planar complexes. *Spectrochim. Acta, Part A* **1991**, *47*, 1263−1268.
(36) Basile, L. J. *Metal-Nitrogen Vibrations*; Springer: US, 1971; pp 191−246.
(37) Assumpção, M.; De Souza, R. F. B.; Rascio, D. C.; Silva, J. C. M.; Calegaro, M. L.; Gaubeur, I.; Paixão, T. R. L. C.; Hammer, P.; Lanza, M. R. V.; Santos, M. C. A comparative study of the electrogeneration of hydrogen peroxide using Vulcan and Printex carbon supports. *Carbon* **2011**, *49*, 2842−2851.
(38) Scarano, D.; Bertarione, S.; Spoto, G.; Zecchina, A.; Otero Areán, C. FTIR spectroscopy of hydrogen, carbon monoxide, and methane adsorbed and co-adsorbed on zinc oxide. *Thin Solid Films* **2001**, *400*, 50−55.
(39) Nandenha, J.; Fontes, E. H.; Piasentin, R. M.; Fonseca, F. C.; Neto, A. O. Direct oxidation of methane at low temperature using Pt/C, Pd/C, Pt/C-ATO and Pd/C-ATO electrocatalysts prepared by sodium borohydride reduction process. *J. Fuel Chem. Technol.* **2018**, *46*, 1137−1145.
(40) Nandenha, J.; Piasentin, R. M.; Silva, L. M. G.; Fontes, E. H.; Neto, A. O.; de Souza, R. F. B. Partial oxidation of methane and generation of electricity using a PEMFC. *Ionics* **2019**, *25*, 5077−5082.
(41) Christensen, P. A.; Linares-Moya, D. The Role of Adsorbed Formate and Oxygen in the Oxidation of Methanol at a Polycrystalline Pt Electrode in 0.1 M KOH: An In Situ Fourier Transform Infrared Study. *J. Phys. Chem. C* **2010**, *114*, 1094−1101.
(42) Fang, X.; Wang, L.; Shen, P. K.; Cui, G.; Bianchini, C. An in situ Fourier transform infrared spectroelectrochemical study on ethanol electrooxidation on Pd in alkaline solution. *J. Power Sources* **2010**, *195*, 1375−1378.
(43) Fontes, E. H.; Piasentin, R. M.; Ayoub, J. M. S.; da Silva, J. C. M.; Assumpção, M. H. M. T.; Spinacé, E. V.; Neto, A. O.; de Souza, R. F. B. Electrochemical and in situ ATR-FTIR studies of ethanol electro-oxidation in alkaline medium using PtRh/C electrocatalysts. *Mater. Renewable Sustainable Energy* **2015**, *4*, No. 3. Scopus.
(44) Zhiani, M.; Majidi, S.; Rostami, H.; Taghiabadi, M. M. Comparative study of aliphatic alcohols electrooxidation on zero-valent palladium complex for direct alcohol fuel cells. *Int. J. Hydrogen Energy* **2015**, *40*, 568−576.
(45) Jin, Z.; Wang, L.; Zuidema, E.; Mondal, K.; Zhang, M.; Zhang, J.; Wang, C.; Meng, X.; Yang, H.; Mesters, C.; Xiao, F. S. Hydrophobic zeolite modification for in situ peroxide formation in methane oxidation to methanol. *Science* **2020**, *367*, 193−197.

https://doi.org/10.1021/acsomega.2c01463
ACS Omega 2022, 7, 24249−24255